Available online at www.sciencedirect.com
ScienceDirect
Polymer 48 (2007) 1176–1184
polymer
www.elsevier.com/locate/polymer

Polymer Communication

Inorganic–organic interpenetrating polymer networks involving polyhedral oligomeric silsesquioxane and poly(ethylene oxide)

Jiangfeng Mu, Yonghong Liu, Sixun Zheng*

Department of Polymer Science and Engineering, Shanghai Jiao Tong University, 800 Dongchuan Road, Shanghai 200240, PR China

Received 2 August 2006; received in revised form 27 December 2006; accepted 6 January 2007
Available online 11 January 2007

Abstract

A novel organic–inorganic interpenetrating polymer network (IPN) was prepared *via in situ* crosslinking between octa(propylglycidyl ether) polyhedral oligomeric silsesquioxane (OpePOSS) and 2,2-bis(4-hydroxyphenyl)propane in the presence of poly(ethylene oxide) (PEO). The miscibility and intermolecular specific interactions of the IPNs were investigated by means of differential scanning calorimetry (DSC), transmission electron microscopy (TEM) and Fourier transform infrared (FTIR) spectroscopy. In view of the results of calorimetric analysis and morphological observation, it is judged that the components of the organic–inorganic IPNs are fully miscible. The FTIR spectroscopy shows that there are inter-component hydrogen bonding interactions between the POSS network and PEO. The measurements of static contact angle show that the hydrophilicity (and/or the surface free energy) of the organic–inorganic IPNs increased with the addition of the miscible and water-soluble polymer (*i.e.*, PEO). Thermogravimetric analysis (TGA) shows that the thermal stability of the IPNs was quite dependent on the mass ratios of the POSS network to PEO.

Keywords: Interpenetrating polymer networks; POSS; Poly(ethylene oxide)

1. Introduction

Interpenetrating polymer networks (IPNs) are defined as the association of two or more polymers that are separately crosslinked into interlocked networks without chemical bonds between polymer components. Ideally, the interpenetration occurs through physical entanglement of component polymers and the networks are coupled at the molecular level [1–4]. Nonetheless, such crosslinked polymer blends often exhibit phase-separated morphology due to the negligible contribution of entropy (ΔS_m) to free energy of mixing (ΔH_m) unless there are intermolecular specific interactions (*e.g.*, hydrogen bonding) in the systems [5,6]. During the past decades, there has been considerable interest to investigate in IPNs and the great interest in IPNs stems from the potential of designing the materials with a range of properties and generating a synergistic effect on the properties of materials [3,7]. The preparations of IPNs can be carried out by the following two approaches: (i) simultaneous crosslinking and (ii) sequential crosslinking. A simultaneous IPN is formed by polymerizing two different monomers or by using two different polymer chains along with complementary crosslinking agent pairs together in one step. The key to the success of this process is that the two components must polymerize (or crosslink) in a fashion without mutual interference. A sequential IPN can be prepared by polymerizing (or crosslinking) the monomers of one component in the presence of the second polymer (*viz.* linear or crosslinked polymer), in order to form the interpenetration networks. This technique can be employed to prepare a semi-IPN, *i.e.*, the crosslinking of one combination of monomer (or precursors) was performed in the presence of a linear polymer [1–4,7].

The previous investigations are mainly focused on the IPN systems of organic components [8–13]. However, the studies

* Corresponding author. Tel.: +86 21 54743278; fax: +86 21 54741297.
E-mail address: szheng@sjtu.edu.cn (S. Zheng).

0032-3861/$ - see front matter © 2007 Elsevier Ltd. All rights reserved.
doi:10.1016/j.polymer.2007.01.007

on organic–inorganic hybrid IPNs remain largely unexplored although there are some reports on polydimethylsiloxane (PDMS)-based IPNs [13–16]. It is expected that organic–inorganic hybrid IPNs can combine the advantages of organic materials with those of inorganic polymers [13,14]. Polyhedral oligomeric silsesquioxane (POSS) macromers and POSS-containing polymers are emerging as a new technology for accessing organic–inorganic hybrid composites [17–32]. POSS molecules possess nanosized cage-like structures, derived from hydrolysis and condensation of trifunctional organosilanes with a formula of $[RSiO_{3/2}]_n$, $n = 6–12$, where R are various types of organic groups, one or more of which are reactive or polymerizable (Scheme 1). With the reactive R groups, POSS molecules can be introduced into the backbones of polymer chains *via* the formation of covalent bonds between POSS cages and polymer matrices [17–34]. During the past years, there have been extensive reports on the organic–inorganic hybrid thermoplastic (or thermoset) nanocomposites containing POSS. To the best of our knowledge, however, there are no precedent reports on the preparation of POSS-containing organic–inorganic IPNs.

Our interest in preparation of POSS-containing IPN is stimulated by the recent progress in the studies of POSS-containing nanocomposites [35,36]. It is expected that the association of POSS-based networks with organic polymers could provide favorable combination of properties from the inorganic networks and organic polymers. By controlling the formation of the inter-component specific interactions (*viz.* hydrogen bonding interactions), the mixing at the molecular level could be attained between the components. In the present work, the inorganic–organic hybrid IPNs were prepared *via* the crosslinking of octa(propylglycidyl ether) polyhedral oligomeric silsesquioxane (OpePOSS) with 2,2-bis(4-hydroxyphenyl)propane in the presence of poly(ethylene oxide) (PEO). In the backbone of crosslinked POSS networks, there are a great number of hydroxyether structural units, which are potential to form the intermolecular hydrogen bonding interactions with ether oxygen atoms of PEO and thus the miscible IPNs could be obtained. The miscibility of the IPN and the intermolecular specific interactions in the IPNs were investigated by means of differential scanning calorimetry (DSC), Fourier transform infrared (FTIR) spectroscopy and transmission electron microscopy (TEM). The thermal properties of the IPNs were investigated in terms of differential scanning calorimetry (DSC) and thermogravimetric analysis (TGA).

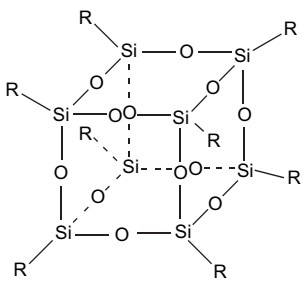

Scheme 1. Structure of polyhedral oligomeric silsesquioxanes.

2. Experimental

2.1. Materials and preparation of samples

2,2-Bis(4-hydroxyphenyl)propane and tetrabutylammonium bromide (TBAB) are of chemically pure grade, purchased from Shanghai Reagent Co., Shanghai, China. Poly(ethylene oxide) (PEO) was supplied by Shanghai Reagent Co., China and it has a quoted molecular weight of $M_n = 20{,}000$. Octa(propylglycidyl ether) polyhedral oligomeric silsesquioxane (OpePOSS) (Scheme 2) was synthesized in this laboratory *via* hydrosilylation of octahydrosilsesquioxane ($H_8Si_8O_8$) with allyl glycidyl ether as detailed elsewhere [31,37].

A desired amount of PEO was added to the stoichiometric mixture of OpePOSS and 2,2-bis(4-hydroxyphenyl)propane. To facilitate the dissolving, a small amount of tetrahydrofuran (10 wt% of reactants) was added to the systems with continuous stirring. The systems were kept at 60 °C for 24 h to evaporate the majority of solvent; the residual solvent was eliminated *in vacuo* at 60 °C for 2 h and the homogenous and transparent blends were obtained in the range of compositions investigated. Tetrabutylammonium bromide (TBAB) (0.1 wt% of reactants) was used as a catalyst and added to the system. The samples were cured at 80 °C for 2 h and at 180 °C for 4 h to access the complete reaction.

2.2. Measurement and techniques

2.2.1. Fourier transform infrared (FTIR) spectroscopy

The FTIR measurements were performed on a Perkin–Elmer Paragon 1000 Fourier transform spectrometer. The spectra were obtained at the resolution of 2 cm^{-1} and were averages of 64 scans. The samples were granulated and the powder was mixed with KBr and then pressed into small flakes for FTIR measurement. All the specimens were sufficiently thin to be within a range where the Beer–Lambert law is obeyed.

2.2.2. Differential scanning calorimetry (DSC)

A Perkin–Elmer Pyris 1 differential scanning calorimeter (DSC) was used to determine thermal transitions. The instrument was calibrated with standard indium. A heating rate of 20 °C/min was used in all cases. To remove the thermal history of the samples, a thermal pretreatment was used. All samples (about 10 mg in weight) were heated up to 180 °C and held for 3 min, and then quenched to −70 °C. The DSC curves were recorded at a heating rate of 20 °C/min. The glass transition temperatures were taken as the midpoint of heat capacity change. The crystallization temperatures (T_c) and the melting temperatures (T_m) were taken as the temperatures of the minima and the maxima of both exothermic and endothermic peaks, respectively.

2.2.3. Transmission electron microscopy (TEM)

Transmission electron microscopy (TEM) was performed on a JEOL JEM-2010 high-resolution transmission electron

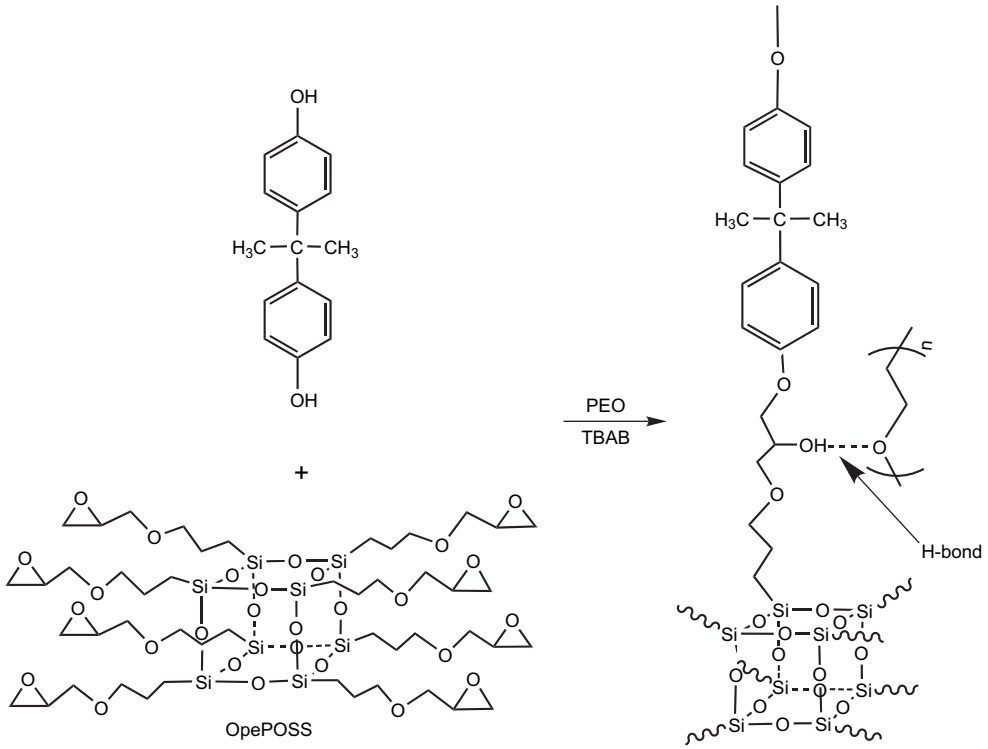

Scheme 2. Preparation of organic–inorganic IPNs involving POSS and PEO.

microscope at an acceleration voltage of 120 kV. The samples were trimmed using an ultrathin microtome machine. The specimen sections (*ca.* 70 nm in thickness) were placed in 200 mesh copper grids for observations.

2.2.4. Contact angle measurements

The specimens for the measurement of contact angle were prepared *via* solution cast techniques. The THF solutions of the mixtures composed of OpePOSS, 2,2-bis(4-hydroxyphenyl)propane and PEO were cast on glass sliders and the thickness of films was controlled to about 20 μm. The solvent was evaporated at room temperature and the residual solvent was eliminated *in vacuo* for 48 h before the samples were cured. The flat free surfaces of the IPNs were used for the measurement of contact angle. The static contact angle measurements with ultra-pure water (H_2O) and diiodomethane (CH_2I_2) were carried out with a KH-01-2 contact angle measurement instrument (Beijing Kangsente Scientific Co., China) at room temperature. The specimens were dried in a vacuum oven for 12 h prior to measurement.

2.2.5. Thermogravimetric analysis (TGA)

A Perkin–Elmer thermal gravimetric analyzer (TGA-7) was used to investigate the thermal stability of the hybrids. The samples (about 5 mg) were heated under air atmosphere from ambient temperature to 900 °C at the heating rate of 20 °C/min in all cases. The thermal degradation temperature was taken as the onset temperature at which 5 wt% of weight loss occurs.

3. Results and discussion

3.1. Preparation of inorganic–organic IPNs

The POSS networks were obtained on the basis of the crosslinking reaction of octa(propylglycidyl ether) polyhedral oligomeric silsesquioxane (OpePOSS) with the stoichiometric amount of 2,2-bis(4-hydroxyphenyl)propane as illustrated in Scheme 2. Catalyzed with tetrabutylammonium bromide (TBAB), the phenol–epoxide reaction can be stoichiometrically carried out at elevated temperature (*e.g.*, 180 °C) [37–39]. Shown in Fig. 1 are the FTIR spectra of OpePOSS,

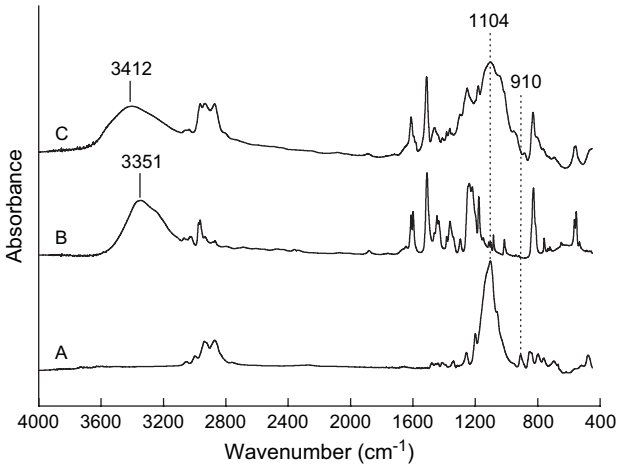

Fig. 1. The FTIR spectra of OpePOSS (A), 2,2-bis(4-hydroxyphenyl)propane (B) and the reacted products of OpePOSS and 2,2-bis(4-hydroxyphenyl)-propane stoichiometric mixture (C).

2,2-bis(4-hydroxyphenyl)propane and the POSS networks. In the FTIR spectrum of OpePOSS, the band at 1109 cm^{-1} is assigned to the stretching vibration of Si–O–Si units in the silsesquioxane cage whereas the band at 910 cm^{-1} is ascribed to the stretching vibration of epoxide groups (Curve A). 2,2-Bis(4-hydroxyphenyl)propane is characterized by the stretching vibration at 3351 cm^{-1}, which is assigned to the band of phenolic hydroxyls (Curve B). Under the present condition, the reaction between OpePOSS and 2,2-bis(4-hydroxyphenyl)-propane afforded a crosslinked product, the FTIR spectrum of which is shown in Fig. 1 (Curve C). It is seen that the band of epoxide group for OpePOSS was virtually depleted, suggesting that the crosslinking reaction was performed to completion. In addition, the hydroxyl stretching vibration is found to shift to a higher frequency at 3412 cm^{-1}. This observation could be attributed to the occurrence of the crosslinking reaction between phenolic hydroxyl and epoxide groups, which results in the formation of a hydroxyether structural unit [–O–CH_2–CH(OH)–CH_2–O–]. In another words, the phenolic hydroxyls of 2,2-bis(4-hydroxyphenyl)propane was converted into secondary alcohol hydroxyl groups since the stretching vibration of secondary alcohol hydroxyl groups occurs at the frequencies higher than that of phenolic hydroxyl groups.

All the ternary mixtures comprising OpePOSS, PEO and 2,2-bis(4-hydroxyphenyl)propane are homogenous and transparent, implying that the mixtures are miscible. The miscibility (or solubility) was ascribed to the non-negligible entropic contribution of mixing (ΔS_m) to free energy of mixing (ΔG_m) since the molecular weights of OpePOSS and 2,2-bis(4-hydroxyphenyl)propane are quite low. At elevated temperature, the crosslinking reaction between OpePOSS and 2,2-bis(4-hydroxyphenyl)propane was initiated. With the crosslinking reaction proceeding, the ternary mixtures were gradually converted into the binary interpenetrating polymer networks composed of 2,2-bis(4-hydroxyphenyl)propane-crosslinked POSS and PEO. The degree of crosslinking reaction was investigated by means of FTIR. Shown in Fig. 2 are the FTIR spectra of the POSS networks and its IPNs containing PEO in the range of 1800–400 cm^{-1}. It is seen that the absorption of epoxide group at 910 cm^{-1} was disappeared for each sample, indicating that the crosslinking reaction between OpePOSS and 2,2-bis(4-hydroxyphenyl)propane has also occurred to completion in the presence of PEO. It should be pointed out that the band at 1300 cm^{-1} is ascribed to the stretching vibration of C–O bond. The increase of intensity for this band results from the increase of PEO content in the IPNs. Therefore, it is plausible to propose that the crosslinking products are the binary IPNs composed of the POSS network and PEO.

3.2. Thermal transitions and morphology

All the organic–inorganic networks are homogenous and transparent at room temperature when the content of PEO is less than 20 wt%. The samples with PEO more than 20 wt% were cloudy owing to crystallization of PEO. It was seen

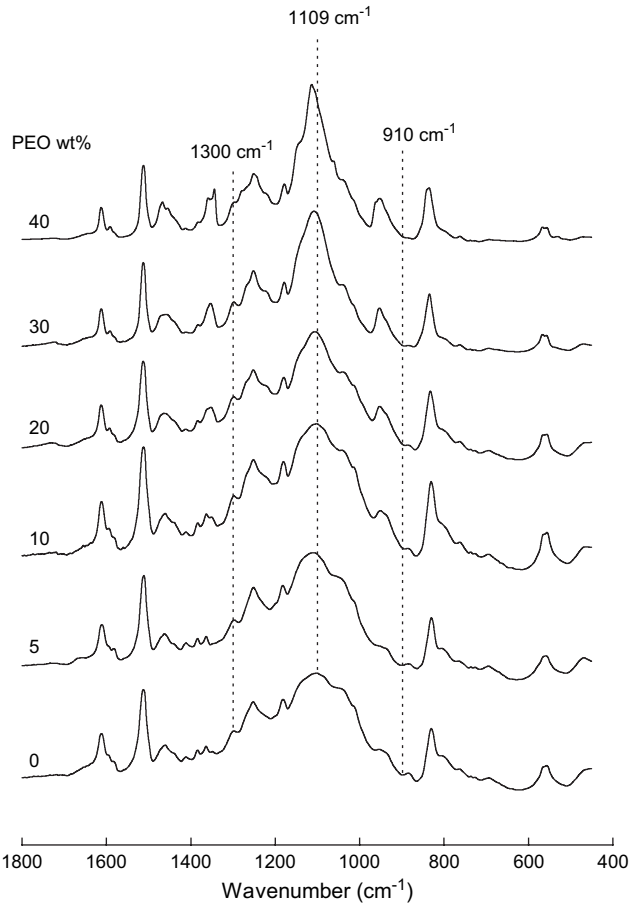

Fig. 2. The FTIR spectra of the POSS network and its IPNs containing PEO in the range of 1800–400 cm^{-1}.

that the cloudy samples became transparent while heated up to 80 °C (*viz*. above the melting point of PEO). The transparency indicates that the organic–inorganic networks present single, homogenous, amorphous phase, *i.e*., no phase separation occurs at least on a scale exceeding the wavelength of visible light. All the networks were subjected to thermal analysis, and the DSC curves are shown in Fig. 3 and the thermal transitions are summarized in Table 1. It is seen that for the control POSS network a glass transition temperature (T_g) at *ca*. 60 °C is discernible although the magnitude of the transition is quite weak. The weak magnitude of glass transition is characteristic of POSS-containing polymers [19–21,31,34], which was responsible for the nanoreinforcement of POSS cages on organic portion of the POSS-containing networks. Upon adding PEO, the magnitude of the transition is increased and the T_gs of the inorganic–organic IPNs shifted to the lower temperature with increasing the concentration of PEO. From Fig. 3, it can be seen that each sample displayed a single glass transition temperature (T_g), intermediate between those of the two pure components and varying with the composition, suggesting that the organic–inorganic networks presented the homogenous amorphous phases. In view of the single glass transition behavior, it is concluded that the POSS networks are fully miscible with PEO in amorphous phase. There are several empirical equations that can describe the

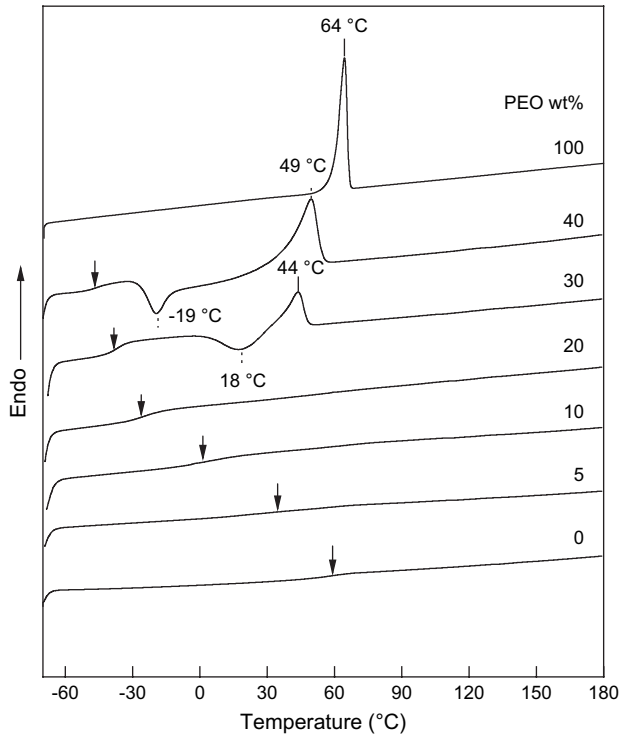

Fig. 3. The DSC thermograms of the POSS network and its IPNs containing PEO.

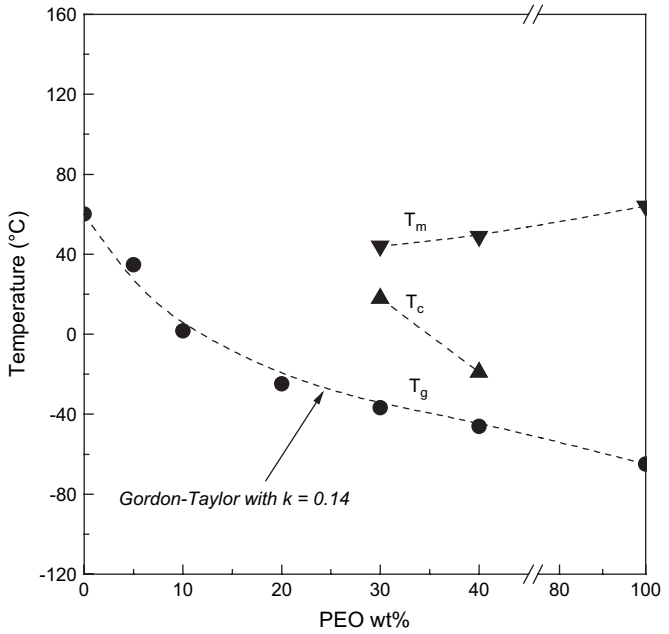

Fig. 4. The plots of glass transition temperature (T_g), crystallization temperature (T_c) and melting temperature (T_m) as functions of PEO content for the inorganic–organic IPNs.

T_g-composition behavior of polymer blends [40–43]. In this work, we use Gordon–Taylor equation [41] to account for the T_g-composition behavior:

$$T_g = \left[\left(W_1 T_{g1} + kW_2 T_{g2}\right)/\left(W_1 + kW_2\right)\right] \quad (1)$$

where k is an adjusting parameter related to the degree of curvature of the T_g-composition curve. It has been proposed that k can be taken as a semi-quantitative measure of miscibility and strength of the intermolecular interaction between components of polymer blends [43–45]. When such an approach is applied to the present organic–inorganic binary IPNs, we obtained a k value of 0.14, fitting the experimental data quite well (see Fig. 4). It is interesting to note that k value is significantly much lower than those obtained for the 1,3,5-trihydroxybenzene-cured blends of epoxy resin and PEO [46–48] although the latter also possesses hydroxyether structural units. The decreased k value could be responsible for the inclusion of silsesquioxane structural units, which itself possess the lower miscibility with PEO.

Returning to Fig. 3, it is noted that the inorganic–organic hybrid composites with PEO less than 20 wt% did not display any crystallinity although PEO is a typical crystalline polymer. This result indicates that PEO chains have been trapped in the POSS networks, *i.e.*, the semi-interpenetrating polymer networks were formed. Nonetheless, the phenomenon of cold crystallization was observed while the content of PEO exceeds 20 wt%. The inorganic–organic networks containing 30 and 40 wt% PEO concurrently displayed the transitions of crystallization and melting. Moreover, the crystallization temperatures (T_cs) of PEO in the IPNs increased with increasing the content of the POSS networks, suggesting that the crystallization of PEO becomes progressively difficult in the inorganic–organic networks. By comparing the enthalpic values of crystallization with those of melting (see Table 1), it is judged that the amorphous samples were obtained when the samples were quenched from elevated temperatures (*e.g.*,

Table 1
Thermal properties of POSS network and its IPNs containing PEO

PEO (wt%)	T_g (°C)	T_c (°C)	T_m (°C)	ΔH_m (J/g)	ΔH_c (J/g)	T_d (°C)	Ceramic yieldth (%)	Ceramic yield^{exp} (%)
0	60.2					321.4	42.7	43.0
5	34.8					313.8	39.5	39.7
10	1.8					286.3	36.5	36.7
20	−24.8					294.8	30.7	30.7
30	−36.8	18.2	44.0	332.0	327.0	299.6	25.6	25.0
40	−46.1	−19.0	49.0	170.1	168.4	260.3	19.2	18.4
100	−65[a]	–	64	205[a]	–	ND	–	–

ND: not detected. Ceramic yieldth: the ceramic yield calculated in term of POSS content. Ceramic yield^{exp}: experimental ceramic yield.
[a] The values taken from Ref. [62].

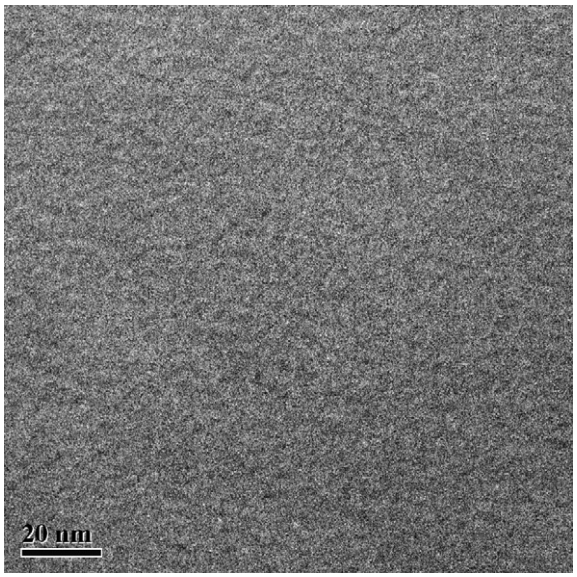

Fig. 5. The TEM micrographs of the inorganic–organic IPNs containing 10 wt% PEO.

180 °C). In addition, it is seen that the melting temperature (T_m) of PEO in the IPNs containing 30 and 40 wt% of PEO is 44 and 49 °C, respectively, which is much lower than that of PEO (64 °C), *i.e.*, the T_m significantly decrease with increasing the contents of the POSS network. The melting point depression of the crystalline component in the IPNs indicates that there is a negative intermolecular interaction parameter (χ_{12}) between the POSS network and PEO, *i.e.,* the IPN system is fully miscible [49,50].

The miscibility was further confirmed with morphological observation. The morphology of the organic–inorganic IPN networks was examined by means of transmission electron microscopy (TEM). Shown in Fig. 5 are the TEM micrographs of the IPN containing 10 wt% of PEO. It is seen that the IPN exhibited the homogenous morphology except there are some compositional inhomogeneity at the nanometer scale. The TEM results indicate that the organic–inorganic IPNs were homogenous at the nanometer scale.

3.3. Intermolecular specific interactions

In view of the structures of POSS network and PEO, it is expected that there could be intermolecular hydrogen bonding between POSS networks and PEO. The ether oxygen atoms of PEO are potential to form the intermolecular hydrogen bonding interactions with the secondary hydroxyls of POSS networks, which can readily be detected by means of infrared spectroscopy. Shown in Fig. 6 are the FTIR spectra of the POSS networks and its IPNs containing PEO in the range of 3000–3800 cm^{-1}. In this region, the spectroscopic bands are ascribed to the hydroxyl stretching vibration. A ramp band at 3438 cm^{-1} was observed for PEO, which is assignable to the stretching vibration of terminal hydroxyl groups of the polymer. For the POSS network, the very broad band centered at 3412 cm^{-1} was attributed to the self-associated hydroxyls

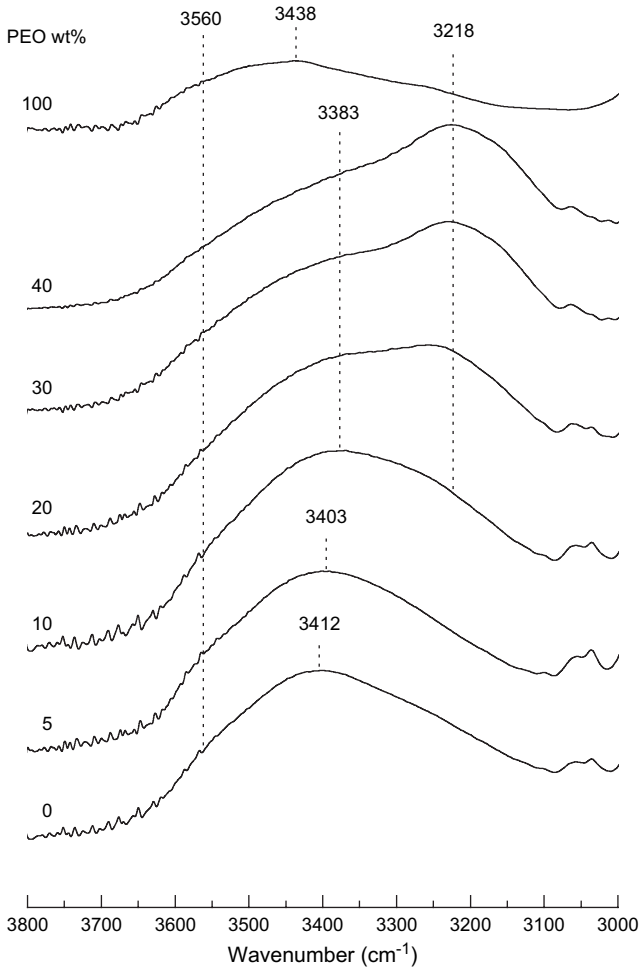

Fig. 6. The FTIR spectra of the POSS network and its IPNs containing PEO in the range of 3800–3000 cm^{-1}.

and the width of the band reflects the broad distribution of hydrogen-bonded hydroxyl stretching frequencies. The shoulder bands centered at 3560 cm^{-1} are ascribed to the stretching vibration of free hydroxyls. Upon adding PEO to the POSS networks, it is seen that the broad hydrogen-bonded hydroxyl bands shifted to the lower frequencies. It is noted that when the content of PEO is more than 10 wt%, a new component of band appeared at 3218 cm^{-1}. The intensity of the band increased with increasing the concentration of PEO. This band could be ascribed to the stretching vibration of the hydroxyl groups that are hydrogen bonded with ether oxygen atom of PEO. Therefore, the population of the hydroxyl groups that H-bonded with PEO is increased with increasing the concentration of PEO. It has been proposed that the frequency difference ($\Delta\nu$) between the free and H-bonded hydroxyls is a measure of the average strength of the intermolecular interactions [51–53]. For the control POSS network, the $\Delta\nu$ value is 148 cm^{-1} for the self-association of hydroxyl groups, while the value of $\Delta\nu = 342$ cm^{-1} is found for the intermolecular hydrogen bonding interactions between the hydroxyl groups of the POSS networks and ether oxygen atoms of PEO. The fact that the stretching vibration bands of the hydrogen-bonded hydroxyls shifted to the lower frequencies indicates

the formation of intermolecular hydrogen bonding between POSS network and PEO, and the intermolecular hydrogen bonding strength in the IPNs is much stronger than the self-association of hydroxyls in the control POSS networks [53,54]. It should be pointed out that the nanoreinforcement of POSS cages could affect the degree of association between the POSS networks and PEO by affecting the molecular dynamics in the composite system [55–57].

3.4. Surface properties

As an organosilicon polymer, the POSS network could possess low surface energy and display the hydrophobicity. It is of interest to examine the change in hydrophobicity (or hydrophilicity) of the materials resulting from the inclusion of a miscible and water-soluble component. The surface properties of the organic–inorganic IPNs were investigated in terms of the measurement of static contact angle. The contact angles were measured with water and diiodomethane as probe liquids, respectively, and the results are summarized in Table 2. The contact angle of the control POSS network was estimated with water to be *ca.* 96.6°, suggesting that the polymer is quite hydrophobic. Upon adding PEO to the system, the contact angles are decreased, implying that the hydrophilicity of the materials was enhanced. Nonetheless, it is noted that there is only a slight decrease in water contact angle when the content of PEO is less than 30 wt%, implying that the POSS component dominates on the surface of the IPN materials, *i.e.,* the POSS moiety on the surface acts as a screening agent to the PEO component. The screening effect was abruptly weakened when the content of PEO exceeds 30 wt% (see Fig. 7). The surface free energies of the hybrid nanocomposites containing various percentages of PEO were calculated according to the geometric mean model [58,59]:

$$\cos\theta = \frac{2}{\gamma_L}\left[\left(\gamma_L^d\gamma_s^d\right)^{1/2} + \left(\gamma_L^p\gamma_s^p\right)^{1/2}\right] - 1 \quad (2)$$

$$\gamma_s = \gamma_s^d + \gamma_s^p \quad (3)$$

where θ is the contact angle and γ_L is the liquid surface tension; γ_s^d and γ_s^p are the polar and dispersive components of γ_L, respectively. From Table 2, it is seen that the total surface free energies of the composites were increased from 32 to 40 mN m^{-1} with increasing the content of PEO. It is noted that the polar component is very sensitive to the concentration of PEO, suggesting that the inclusion of PEO moiety significantly increased the distribution of the polar groups (*i.e.*, ethylene oxide unit) on the surface energy of materials, *i.e.*, the distribution of PEO chains on the surface was increased. This result suggests that the hydrophilicity of the organic–inorganic IPNs can be increased by adding the miscible and water-soluble polymer (*i.e.*, PEO).

Table 2
Static contact angles and surface free energy of IPNs involving POSS and PEO

PEO (wt%)	θ_{H_2O} (°)	$\theta_{CH_2I_2}$ (°)	γ_s^d (mN m^{-1})	γ_s^p (mN m^{-1})	γ_s (mN m^{-1})
0	96.56	54.87	31.52	0.70	32.22
5	93.50	52.63	32.80	1.07	33.86
10	91.77	52.75	32.73	1.42	34.15
20	90.29	51.53	33.42	1.65	35.06
30	89.57	48.17	35.29	1.54	36.83
40	77.79	42.30	38.43	4.46	42.90

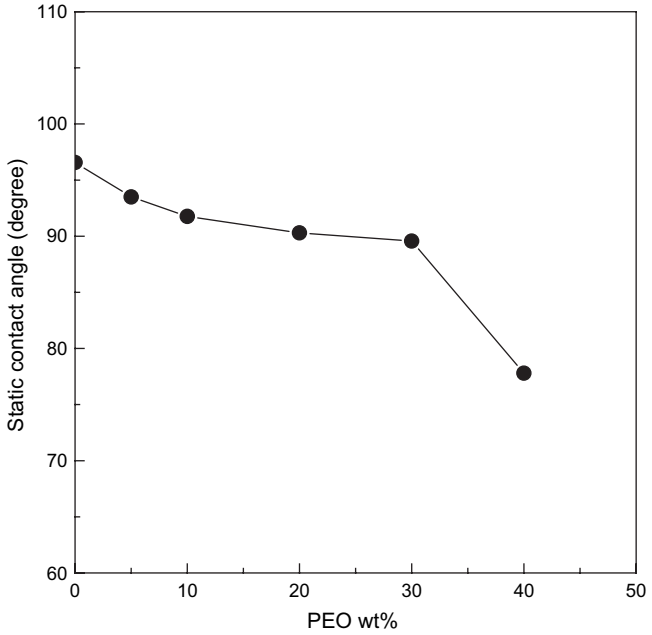

Fig. 7. The plot of water contact angle as a function of PEO content for the organic–inorganic IPNs.

3.5. Thermal stability

Thermogravimetric analysis (TGA) was applied to evaluate the thermal stability of the control POSS network and its IPNs containing PEO. Shown in Fig. 8 are the TGA curves of the control POSS network and its IPNs containing PEO, recorded in an air atmosphere at a heating rate of 20 °C/min and the results are summarized in Table 1. Within the experimental temperature range, all the samples displayed similar degradation profiles, suggesting that the existence of PEO did not significantly alter the degradation mechanism of the matrix networks. For the control POSS network, initial decomposition occurred at *ca.* 321 °C and the summation of char and ceramic yields was found to be 42.7 wt%. In terms of the theoretical ceramic content, it is judged that no char yield was obtained for the decomposition of the control POSS network under the present condition. For the organic–inorganic IPNs, it is noted that the T_ds of the organic–inorganic IPNs reduced with inclusion of the organic component (*viz.* PEO) and decreased with increasing the content of PEO. In addition to the decreased initial decomposition temperature, it is also noted that the rates of weight loss from segmental decomposition were significantly increased. By comparing the theoretical ceramic yields with those experimental obtained (see Table 1), it is judged that no char was formed during the decomposition of the POSS network and the IPNs containing PEO, *i.e.*, all the

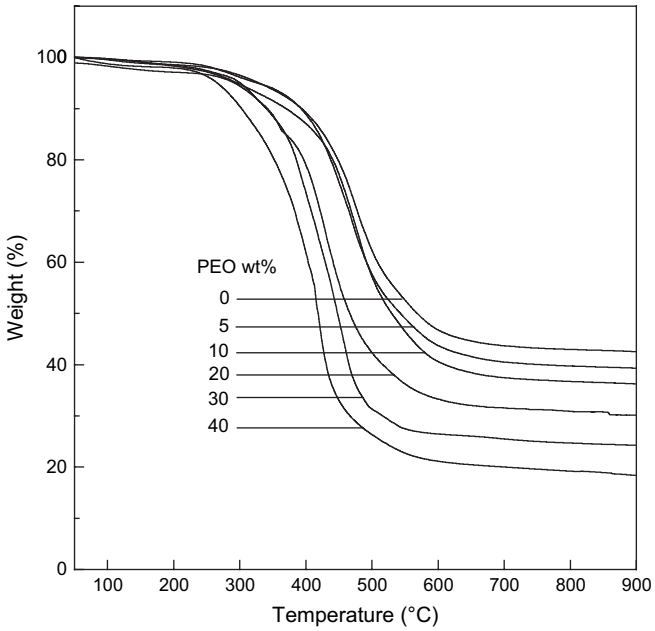

Fig. 8. The TGA curves of the POSS network and its IPNs containing PEO.

organic portions in the inorganic–organic IPNs were fully decomposed. This result is in a marked contrast to those obtained in layered silicates-containing polymer nanocomposites [60,61].

4. Conclusions

A new type of organic–inorganic interpenetrating polymer networks (IPNs) were prepared *via in situ* crosslinking between octa(propylglycidyl ether) polyhedral oligomeric silsesquioxane (OpePOSS) and 2,2-bis(4-hydroxyphenyl)propane in the presence of poly(ethylene oxide) (PEO). The miscibility and intermolecular specific interactions of the IPNs were investigated by means of differential scanning calorimetry (DSC), transmission electron microscopy (TEM) and Fourier transform infrared (FTIR) spectroscopy. Both single, composition-dependent glass transition behavior and homogenous morphology indicate that the components of the organic–inorganic IPNs are fully miscible and there are inter-component hydrogen bonding interactions between the crosslinked POSS networks and PEO. The organic–inorganic composite networks displayed single, composition-dependent glass transition temperatures (T_gs). Thermogravimetric analysis (TGA) shows that the thermal stability of the IPNs was quite dependent on the mass ratios of the POSS network to PEO. The surface hydrophilicity (and/or the surface free energy) of the organic–inorganic IPNs is quite dependent on the content of the miscible and water-soluble polymer (*i.e.*, PEO).

Acknowledgments

This financial support from Shanghai Science and Technology Commission, China under a key project (No. 02DJ14048) was acknowledged. The authors also would like to acknowledge Natural Science Foundation of China (Project No. 20474038 & 50390090) and Shanghai Educational Development Foundation, China under an Award (2004-SG-18) to "Shuguang Scholar" for the partial support.

References

[1] Sperling LH. Interpenetrating polymer networks and related materials. New York: Plenum Press; 1981.
[2] Klempner D, Sperling LH, Utracki LA, editors. Interpenetrating polymer networks. Advances in chemistry series, vol. 239. Washington, DC: ACS; 1994.
[3] Sperling LH, Mishra V. Adv Polym Technol 1996;7:197.
[4] Hourston DJ, Schafer FU. Polymer 1996;37:3521.
[5] Pascault JP, Williams RJJ. In: Paul DR, Bucknall CB, editors. Polymer blends, vol. 1. New York: Wiley; 2000. p. 379–415.
[6] Guo Q. In: Shonaik GO, Simon G, editors. Polymer blends and alloy. New York: Marcel Dekker; 1999. p. 155–87 [chapter 6].
[7] Yoo SH, Cohen C, Hui C-Y. Polymer 2006;47:6226.
[8] Vancaeyzeele C, Ficht O, Amana B, Boileau S, Teyssie D. Polymer 2006; 47:6048.
[9] Plesse C, Vidal F, Randriamahazaka H, Teyssie D, Chevrot C. Polymer 2005;46:7771.
[10] Nowers JR, Narasimhan B. Polymer 2006;47:1108.
[11] Vancaeyzeele C, Fichet O, Laskar J, Boileau S, Teyssie D. Polymer 2006; 47:2046.
[12] Vidal F, Fichet O, Laskar J, Teyssie D. Polymer 2006;47:3747.
[13] Vancaeyzeele C, Fichet O, Amana B, Boileau S, Teyssie D. Polymer 2006;47:6048.
[14] Clarson SJ, Fitzgerald JJ, Owen MJ, Smith SD. Silicones and silicone-modified materials. In: ACS symposium series, vol. 729. Washington, DC; 2000.
[15] Mark JE, Ning YP. Polym Eng Sci 1985;25:824.
[16] Fichet O, Vidal F, Laskar J, Teyssie D. Polymer 2005;46:37.
[17] Feher FJ, Wyndham KD, Baldwin RK, Soulivong D, Lichtenhan JD, Ziller JW. Chem Commun 1999;1289.
[18] Feher FJ, Wyndham KD, Soulivong D, Nguyen F. J Chem Soc Dalton Trans 1999;1491.
[19] Lichtenhan JD, Vu NQ, Carter JA, Gilman JW, Feher FJ. Macromolecules 1993;26:2141.
[20] Lichtenhan JD, Otonari YA, Carr MJ. Macromolecules 1995;28:8435.
[21] Lee Y-J, Kuo S-W, Huang C-F, Chang F-C. Polymer 2006;47:4378.
[22] Haddad TS, Lichtenhan JD. Macromolecules 1996;29:7302.
[23] Lee Y-J, Kuo S-W, Su Y-C, Chen J-K, Tu C-W, Chang F-C. Polymer 2004;45:6321.
[24] Wright ME, Schorzman DA, Feher FJ, Jin R-Z. Chem Mater 2003;15: 264.
[25] Choi J, Harcup J, Yee AF, Zhu Q, Laine RM. J Am Chem Soc 2001;123: 11420.
[26] Choi J, Kim SG, Laine RM. Macromolecules 2004;37:99.
[27] Mya KY, He C, Huang J, Xiao Y, Dai Y, Siow Y-P. J Polym Sci Part A Polym Chem 2004;42:3490.
[28] Laine RM, Choi J, Lee I. Adv Mater 2001;13:800.
[29] Ni Y, Zheng S. Chem Mater 2004;16:5141.
[30] Liu H, Zheng S, Nie K. Macromolecules 2005;38:5088.
[31] Liu Y, Meng F, Zheng S. Macromol Rapid Commun 2005;26:920.
[32] Mya KY, Li X, Chen L, Ni XP, Li J, He CB. J Phys Chem B 2005;109: 9455.
[33] Kopesky ET, McKinley GH, Cohen RE. Polymer 2006;47:299.
[34] Kopesky ET, Haddad TS, McKinley GH, Cohen RE. Polymer 2005;46: 4743.
[35] Li G, Wang L, Ni H, Pittman CU. J Inorg Organomet Polym 2001;11: 123.
[36] Abe Y, Gunji T. Prog Polym Sci 2004;29:149.
[37] Liu Y, Zheng S. J Polym Sci Part A Polym Chem 2006;44:1168.

[38] Zheng S, Huang J, Zhong Z, He G, Guo Q. J Polym Sci Part A Polym Chem 1999;37:525.
[39] Zheng S, Guo Q, Chan C-M. J Polym Sci Part A Polym Chem 1999;37:2329.
[40] Fox TG. Bull Am Phys Soc 1956;1:123.
[41] Gordon M, Taylor JS. J Appl Chem 1952;2:496.
[42] Couchman PR. Macromolecules 1978;11:1156.
[43] Olabisi O, Robeson LM, Show MT. Polymer–polymer miscibility. New York: Academic Press; 1979.
[44] Belorgey G, Prud'homme RE. J Polym Sci Part B Polym Phys 1982;20:191.
[45] Belorgey G, Aubin M, Prud'homme RE. Polymer 1982;23:1051.
[46] Hu L, Lu H, Zheng S. J Polym Sci Part B Polym Phys 2004;42:2567.
[47] Lu H, Zheng S. J Polym Sci Part B Polym Phys 2005;43:359.
[48] Zheng S, Lu H, Chen C, Guo Q. Colloid Polym Sci 2003;281:1015.
[49] Nishi T, Wang TT. Macromolecules 1975;8:909.
[50] Paul DR, Barlow JW, Bernstein RE, Wahrmund DC. Polym Eng Sci 1978;18:1225.
[51] Purcell KF, Drago RS. J Am Chem Soc 1968;24:251.
[52] Coleman MM, Painter PC. Appl Spectrosc Rev 1984;20:225.
[53] Coleman MM, Graf JF, Painter PC. Specific interactions and the miscibility of polymer blends. Lancaster, PA: Technomic Publishing; 1991.
[54] Coleman MM, Painter PC. Prog Polym Sci 1995;20:1.
[55] Mya KY, Pramoda KP, He CB. Polymer 2006;47:5035.
[56] Bhaharadwaji RK, Berry RJ, Farmer BR. Polymer 2000;41:7209.
[57] Striolo A, McCabe C, Cummings PT. Macromolecules 2005;38:8950.
[58] Kaelble DH, Uy KC. J Adhes 1970;2:50.
[59] Kaelble DH. Physical chemistry of adhesion. New York: Wiley-Interscience; 1971.
[60] Pebaron PC, Wang Z, Pinnavaia TJ. Appl Clay Sci 1999;15:1.
[61] Ray SS, Okamoto M. Prog Polym Sci 2003;28:1539.
[62] Vidotte G, Levy DL, Kovacs AJ. Kolloid Z Z Polym 1969;230:289.